ROYAL SOCIETY
OF CHEMISTRY

PAPER

Check for updates

Exciton dissociation in quantum dots connected with photochromic molecule bridges†

Lucy U. Yoon,[a] Surya B. Adhikari,[b] Ephraiem S. Sarabamoun,[c] Jonathan M. Bietsch,[b] Esther H. R. Tsai,[d] Guijun Wang [ID] *[b] and Joshua J. Choi [ID] *[ac]

We report modulation of exciton dissociation dynamics in quantum dots (QD) connected with photochromic molecules. Our results show that switching the configuration of photochromic molecules changes the inter-QD potential barrier height which has a major impact on the charge tunnelling and exciton dissociation. The switching of the dominant exciton decay pathway between the radiative recombination and exciton dissociation results in switchable photoluminescence intensity from QDs. Implications of our findings for optical memory and optical computing applications are discussed.

Introduction

Quantum dots (QDs) are scientifically intriguing and technologically promising nanoscale building blocks for hierarchical materials with tunable emergent properties.[1–7] A wide range of tunable properties of QDs has been demonstrated, the most prominent being the size-tunable optical properties from programmable atomic-like energy levels[7–9] from which the view of QDs as 'designer atoms' originates. Moreover, in assemblies of multiple QDs, the electronic interaction between adjacent QDs can be viewed as programmable 'designer bonds' because of the tunable inter-QD distances and electronic coupling strengths. Considering that manipulating the structure of QD assemblies is possible by controlling the rich self-assembly behaviors of QDs,[10–15] one can imagine building 'designer QD solids' that give rise to novel properties.[16,17]

Previous studies have shown that the length of the molecules that inter-connect QDs and their end group moieties can have major influence over charge conduction,[18–27] exciton dissociation[28,29] and surface trap densities.[25,27] Most studies so far have been focused on achieving strong electronic coupling required for optoelectronic device applications. To this end,

a variety of short organic molecules such as ethanedithiol,[28,30–32] benzenedithiol,[33] mercaptopropionic acid[29] and thiocyanate[34,35] has been employed. Also, short metal chalcogenide complex ligands[36] have been shown to result in extremely strong inter-CQD electronic coupling.[37] Atomic anions, as the ultimate short ligands, have been demonstrated in CQD solar cells[25] and field-effect transistor devices.[38]

Despite progress in achieving large electronic coupling using short ligands, the microscopic understanding of the impact of physical and electronic structure of bridge molecules on charge transfer and exciton dynamics in QD assemblies is still lacking. To effectively leverage the large library of possible bridge molecules and realize the full potential of QD 'designer solids', a deeper understanding that goes beyond merely tuning the length of bridge molecule is required. Specifically, the effect of changing potential barrier heights through different molecular structure on charge transfer and exciton dynamics in QD assemblies is still poorly understood. This is challenging to study because employing a set of bridge molecules designed to provide different potential barrier height in general will also introduce differences in other key factors such as molecule length and binding groups that have major impact on charge transfer. Moreover, comparing charge transfer behavior in multiple samples with different molecular structures will introduce variability in charge donors and acceptors due to inhomogeneities in QD populations such as different sizes, shapes, and different bonding with molecules.

Here, we report a study that tests a hypothesis that optically switching the configuration and the energy levels of the photochromic bridge molecules will enable tuning of the potential barrier height between the QDs and therefore the charge transfer rate and exciton dynamics (Fig. 1). QDs connected with a configuration of photochromic molecules with large energy gap between highest occupied molecular orbital (HOMO)

[a] *Department of Chemical Engineering, University of Virginia, Charlottesville, VA 22904, USA. E-mail: jjc6z@virginia.edu*

[b] *Department of Chemistry and Biochemistry, Old Dominion University, Norfolk, VA 23529, USA. E-mail: g1wang@odu.edu*

[c] *Department of Physics, University of Virginia, Charlottesville, VA 22904, USA*

[d] *Center for Functional Nanomaterials, Brookhaven National Laboratory, Upton, NY 11973, USA*

† Electronic supplementary information (ESI) available: Syntheses procedure of PCM and mono-esterified PCM, PbS QD synthesis method and optical characterization, absorbance, PL, TR-PL, Raman, and GISAXS results of PCM bridged QD assemblies, 1D and 2D NMR characterizations of synthesized PCMs, PL switching study of PCM treated PbS QD in solution form. See DOI: 10.1039/d1tc04451f
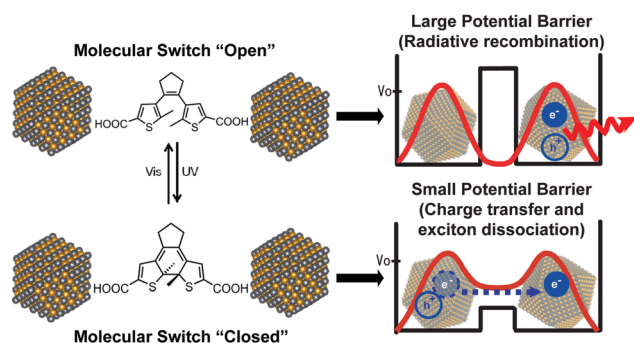
16006 | *J. Mater. Chem. C*, 2021, **9**, 16006–16013

This journal is © The Royal Society of Chemistry 2021

Fig. 1 A schematic showing a mechanism of modulating charge transfer and exciton dissociation in QD assemblies by optically switching the configuration of bridge molecules to change the inter-QD potential barrier heights.

and lowest unoccupied molecular orbital (LUMO) will provide a larger potential barrier height and smaller electronic coupling between the QDs compared to a configuration with a smaller energy gap. A direct consequence of changing inter-QD electronic coupling and the degree of exciton delocalization is different rates of exciton dissociation.[28,29] Our results indeed show that the changing the photochromic molecules' configuration and its associated inter-QD potential barrier height can switch the dominant pathway for the excitons in QDs between radiative recombination or tunnelling induced exciton dissociation (Fig. 1). Our approach of exploiting configuration switching of the photochromic molecules while keeping other key factors constant (exactly identical charge donor–acceptor QD pairs, identical binding at contacts between the molecules and QD surface, *etc.*) is an advantageous method to isolate and study how changing potential barrier height impact inter-CQD exciton dissociation and charge transfer. The switching of the dominant exciton decay pathway between the radiative recombination and exciton dissociation results in switchable photoluminescence (PL) intensity from QDs which can be exploited in optical memory and optical computing applications.

Results and discussion

Dithienylethenes derivatives were chosen as the photochromic molecules in this study for the following reasons: (1) reversible configuration change with ultraviolet or visible light irradiation,[39–43] (2) minimal differences in molecular length between the configurations (~ 1 Å),[40] (3) a large change in HOMO–LUMO energy gap upon configuration change (~ 2 eV)[44] and (4) fast switching speeds of a few picoseconds.[45] As for the QDs, PbS QDs were selected because of their high degree of electronic coupling and low exciton binding energy.[28] This will enable more sensitive detection of change in exciton dissociation.[28] Also importantly, the near-IR absorbance and PL of PbS QDs will allow monitoring of the exciton dynamics in QD assemblies in the range of light wavelength regions that do not disturb the configuration of the dithienylethene molecules.

Specifically, dithienylethenes derivatives with carboxylic acid functional groups (compound **6** in Scheme S1 of the ESI†) were employed for the experiments in this study. From this point on, we will refer to the compound **6** simply as PCM (photochromic molecule). The PCM undergoes a photo-induced transition between its unconjugated open-ring isomer (referred to as an "open" state) and the conjugated closed-ring isomer (a "closed" state) (Fig. 1).[42] The change in electronic transition energies upon the configuration switch can be observed in the absorbance spectra of PCM shown in Fig. 2a. As the configuration switch in the PCM populations progresses, the absorbance spectra show an isosbestic point at 320 nm. Upon exposure at 300 nm wavelength light, the absorbance peaks at 541 nm and 360 nm increase as more PCMs switch to the "closed" configuration. In contrast, irradiating the molecules with 541 nm wavelength light switches PCMs to the "open" state and therefore the absorbance peaks at 541 nm and 360 nm decrease. Based on these results, we selected 300 nm and 541 nm wavelength light to switch the configuration of the PCM to "closed" and "open" state respectively throughout this study.

Three different sizes of PbS QDs were employed for this study (see the ESI† for synthesis method). The size dependent energy gaps of QDs result in different energy levels of HOMO and LUMO, allowing us to systematically tune the potential barrier height with respect to the PCM's energy levels. The absorbance and PL spectra of the synthesized PbS QDs are shown in Fig. 2b and c. Based on the first excitonic peak energy of 1.39 eV, 1.03 eV, and 0.90 eV in the absorbance spectra (Fig. 2b), the diameter of PbS QDs were estimated to be 2.9 nm, 3.6 nm and 4.7 nm respectively, using a sizing curve in the literature.[46] The corresponding PL emission wavelengths for each size are located at 1020 nm, 1200 nm, and 1380 nm, respectively. Fig. 2d shows a plot of corresponding HOMO and LUMO energy levels of PbS QDs and PCM according to the literature.[44] As the QD diameter gets smaller from 4.7 nm to 2.9 nm, the LUMO energy level increases from −4.0 eV to −3.6 eV with respect to the vacuum while the HOMO energy level decreases from −4.9 eV to −5.0 eV. The energy levels of the LUMO in the "closed" and "open" state of PCM are −3.4 eV and −2.1 eV, respectively. Based on these values, the potential barrier height formed by the difference in LUMO energy levels with a closed state of PCM varies from 0.6 eV to 0.2 eV depending on the QD sizes. Additionally, it should be noted that the HOMO–LUMO energy levels of both closed and open state of PCM form type-I alignment[44] with respect to all three QD sizes, indicating that the direct charge transfer[47] from band edge states in QD to the PCM is not likely to occur in either configuration.

The PCM bridged QD assembly samples were prepared in a nitrogen environment glovebox through spin-coating as-synthesized QDs on a cleaned glass slide and performing ligand exchange procedure to replace the native ligands, oleates, with the PCM (see the ESI† for details of the sample preparation method). The carboxylic acid functional groups on both ends of the PCM readily exchange with oleates on the PbS QD surface.[48] After getting bridged and cross-linked by PCMs, the QD assemblies were no longer dispersible in solvents such as

This journal is © The Royal Society of Chemistry 2021

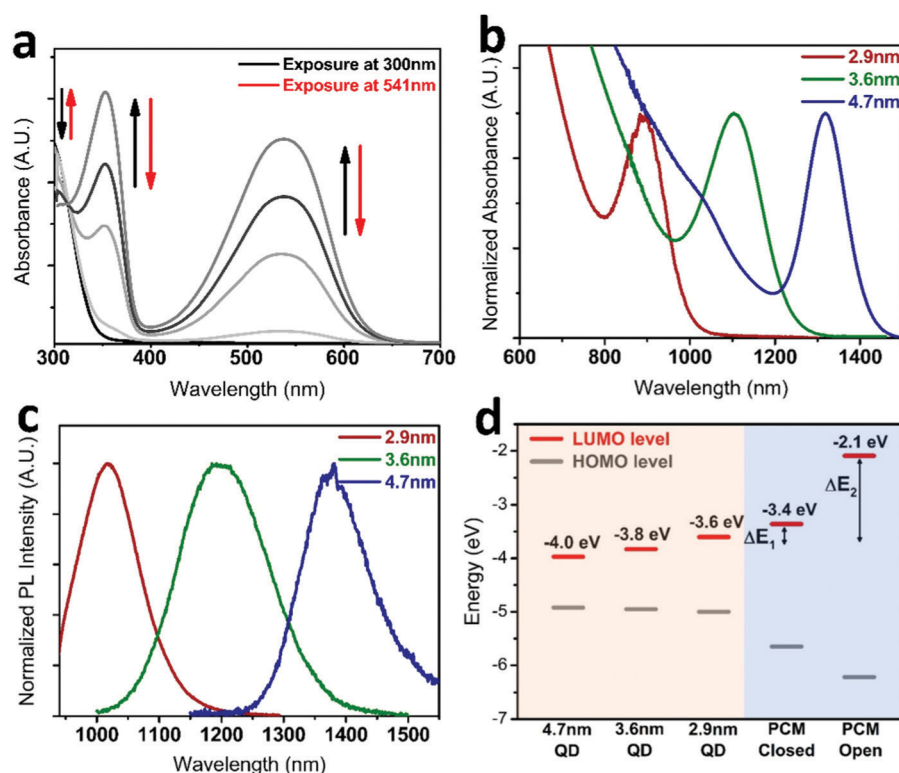*J. Mater. Chem. C*, 2021, **9**, 16006–16013 | **16007**

Fig. 2 (a) Absorbance spectra of PCM in methanol solution after light irradiation at 300 nm or 541 nm to induce configuration switch. (b) Normalized absorbance spectra and (c) PL spectra of PbS QDs with different sizes (2.9 nm, 3.6 nm, and 4.7 nm) used for this study. 750 nm was used as an excitation wavelength. (d) The HOMO−LUMO energy levels of QD with different sizes and PCM with "closed" or "open" configuration.

hexane or toluene. The cross-linking induced solvent orthogonality allowed the ligand exchange procedures to be repeated multiple times with the samples being thoroughly washed in between to remove excess ligand molecules. Raman spectroscopy measurements were performed on the samples to monitor the extent of the ligand exchange. As shown in Fig. S6 (ESI†), peaks at 1425 cm^{-1} and 1550 cm^{-1} correspond to oleate molecules as native ligands on PbS QD surface. As the number of ligand exchange procedure increases, the intensity of these peaks gradually decreases. The sample with three cycles of ligand exchange shows almost a complete elimination of these peaks, indicating that most of the oleate molecules in the QD assembly sample has been exchanged with PCM (Fig. S6, ESI†).

PL measurements were performed to monitor the effect of switching PCM configuration on exciton recombination in QD assemblies (Fig. 3). Samples with QD sizes of 2.9 nm, 3.6 nm, and 4.7 nm were prepared and encapsulated with two glass slides and epoxy around all edges to avoid any potential complications from ambient air exposure during the measurement. First, the samples were irradiated with 300 nm light to switch PCMs to the "closed" state and then PL spectra was taken using 750 nm light irradiation which excites the QDs only without disturbing the PCM state. Afterwards, the samples were exposed to 541 nm light to switch the PCMs to the "open" state after which PL spectra were taken with 750 nm light excitation. It should be noted that 750 nm light employed for PL measurements does not get absorbed by PCMs and photoexcites QDs only. This process was

repeated multiple times to check for cyclability. Additional details of this experimental procedure are described in the ESI.† Fig. 3a–c show that PL intensities from all samples show reversible decrease and increase with the "closed" and "open" PCM state respectively. For 2.9 nm sized QDs, the PL intensity is ∼46% higher with "open" PCM state compared to the "closed" state (Fig. 3a and d). The differences in the PL intensity are considerably smaller for bigger QDs with ∼25% higher for 3.6 nm QDs (Fig. 3b and e) and ∼23% higher for 4.7 nm QDs (Fig. 3c and f) for the "open" PCM state. These results suggest that the different potential barrier heights formed by the offset in energy levels of PCM with QDs of different sizes may be influencing the fractions of excitons that go through inter-CQD dissociation. However, since other key factors such as size dependent properties of QDs, inter-QD distances, etc. that influence exciton recombination dynamics are also different in these samples, further studies are required to delineate them. Repeating the PL measurement cycle results in an alternating PL intensity from QDs indicating that the response in the fraction of excitons undergoing radiative recombination to switching the PCM configuration is a reversible and non-destructive process. The absorbance spectra of the samples with the PCM in "closed" and "open" states (Fig. S7, ESI†) show that there is no noticeable difference due to the configuration switching. Therefore, we conclude that the reversible switching of PL intensity observed in Fig. 3 is not due to irreversible changes in QDs such as degradation and other processes but instead is governed by the structural changes in the PCMs that bridge QDs. It should be noted
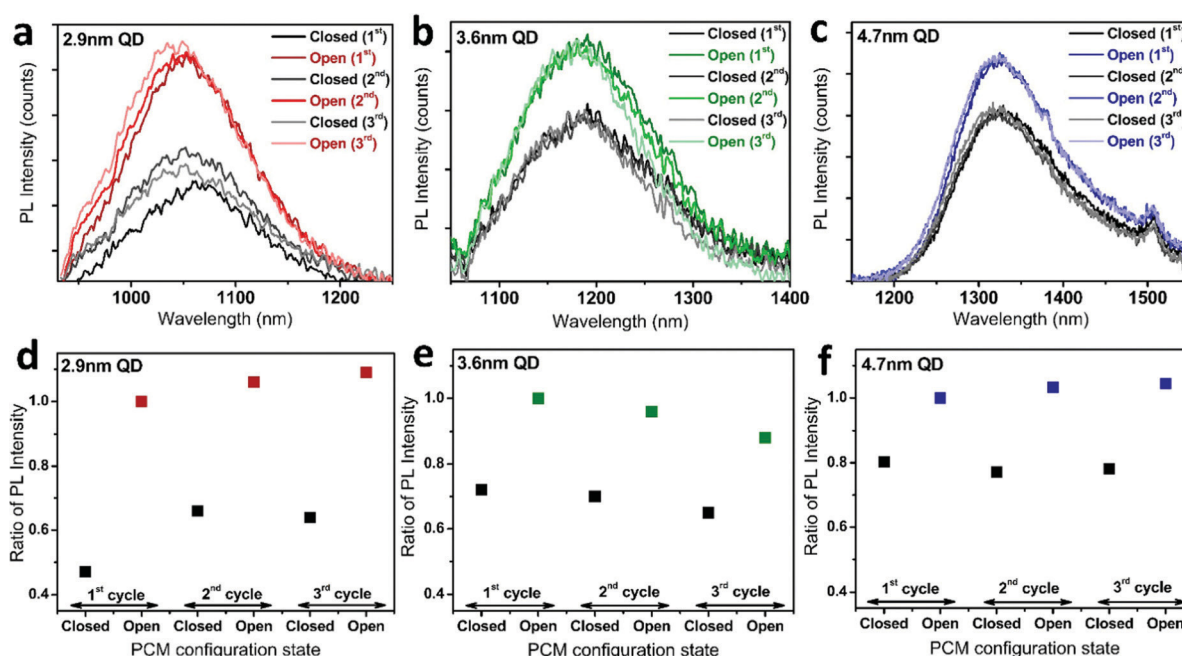
16008 | J. Mater. Chem. C, 2021, 9, 16006–16013

This journal is © The Royal Society of Chemistry 2021

Fig. 3 PL spectra of (a) 2.9 nm, (b) 3.6 nm, and (c) 4.7 nm QD assemblies after the configuration of PCM bridge molecules is switched between "closed" and "open" states. Illumination with 300 nm and 541 nm wavelength light was employed to close and open the PCM configuration, respectively. As a function of repeated cycles of PCM configuration switching, the ratio of PL intensity to the first cycle "open" configuration intensity is plotted for (d) 2.9 nm, (e) 3.6 nm, and (f) 4.7 nm QD assemblies.

that some drifting in PL intensities is observed after repeated cycles of switching PCM state between "open" and "closed" (Fig. 3). This may have been caused by slightly different fraction of switched PCMs in each cycle or degradation of QDs over longer time scale. However, these differences do not change our conclusion as they are significantly smaller compared to the large switches in PL intensity within each cycle due to the PCM configuration change. The precise mechanisms for the slow drift in PL intensity after each cycle are currently being investigated in our laboratories.

To further investigate the nature of the reversible PL intensity switching, we performed time-resolved PL (TR-PL) measurement to gain insights into the exciton decay pathway. Based on the mechanism of exciton delocalization and dissociation through tunneling[28,29] lower potential barrier between QDs due to "closed" PCM state would lead to faster exciton dissociation and decreased PL lifetime. Fig. 4a–c show that PL lifetimes are indeed shorter in QDs when the PCM is in the "closed" state compared to the "open" state. To quantify the lifetimes, bi-exponential decay functions were fitted, and the lifetime values were calculated through weighted averaging of the two terms.[49] Our results show that the 2.9 nm QD assembly shows the biggest differences in the PL lifetimes of 31 ns and 61 ns when the PCMs are in the "closed" and "open" state respectively. The differences in the PL lifetimes in 3.6 and 4.7 nm QD assemblies also show the same trend but to a smaller degree compared to the 2.9 nm QD sample. These trends in PL lifetimes are consistent with the differences in PL spectra intensity as a function of PCM state and QD size (Fig. 3).

The shorter PL lifetime and lower PL intensity of QD assembly with the "closed" PCM state are consistent with our proposed inter-QD exciton dissociation mechanism[28,50] due to lower inter-QD potential barrier height. It is possible that the change in the PL behavior may also draw contributions from any changes in inter-QD distances due to the PCM configuration switch. However, based on the molecular structure of the dithie-nylethene backbone, the PCM employed in this work is expected to have a difference of only ~1 Å in lateral length upon configuration change. To experimentally quantify inter-QD distances with different PCM configurations, we performed grazing incidence small angle X-ray scattering (GISAXS) measurements at the National Synchrotron Light Source II at Brookhaven National Laboratory (see the ESI† for detailed GISAXS measurement method). The GISAXS scattering plots of 2.9 nm QD assemblies with the "open" and "closed" PCM states are shown in Fig. S8a and b (ESI†) and their azimuthally integrated scattering X-ray intensities show peaks that correspond to the periodicity in inter-QD spacing (Fig. S8c and d, ESI†). The inter-QD distance values with the "open" and "closed" PCM state in samples with different QD sizes are summarized in Table S1 (ESI†). The amount of change in measured inter-QD distance between the "open" and "closed" PCM states varies from 0.07 Å to 1.4 Å across different samples. It is likely that the small change of ~1.0 Å in the inter-QD distance change is not the major cause for the observed PL behavior. However, further studies are needed to quantify and delineate contributions from various parameters.

Other possible mechanisms responsible for the observed changes in PL intensity and lifetime are surface charge trapping, Förster resonant energy transfer (FRET)[51–54] to some energy acceptors, and direct charge transfer[47,55,56] from QD to
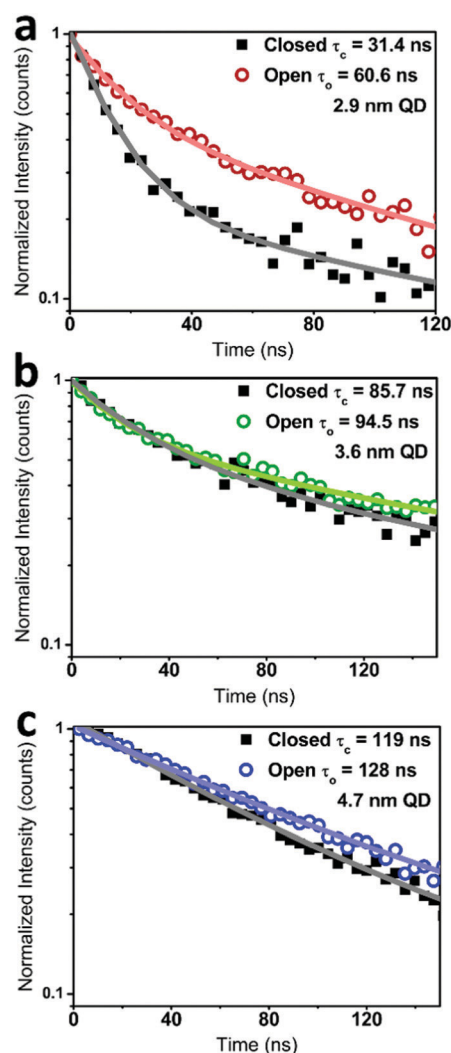

Fig. 4 Time-resolved PL results from (a) 2.9 nm QD, (b) 3.6 nm QD, and (c) 4.7 nm QD assemblies with "open" or "closed" configuration of PCM bridges.

PCM molecules. Based on the fact that the PL and TR-PL measurements were performed on the identical sample wherein the only difference was in the history of light exposure sequence to switch the PCM configuration, we argue that changes in charge trapping amount being responsible for the reversible changes in PL as observed in this work are highly unlikely. As for the FRET mechanism, which is an energy transfer process through dipole–dipole interaction, occurs when there is a resonance in energy between the electronic transitions in the donor and the acceptor. As such, the PL spectra of the QDs need to overlap with the absorption energy of any suitable acceptors nearby. Possible energy acceptors are surface ligands[57–59] and nearby QDs that have not been photoexcited.[28,60,61] As shown in Fig. 2a and c, the light absorption by the PCM occurs in the UV-visible spectrum range which is significantly higher in energy than the near-IR PL of the QDs, indicating that FRET from QDs to PCM is not responsible for the observed PL changes. Also, in our samples, neighbouring QDs are exactly identical before and after the

PCM configuration change and therefore changes in FRET between QDs, if any, will be insignificant. Another possibility is direct charge transfer from QDs to PCM in the "closed" state being responsible for the reduction in PL intensity and lifetime observed in this work. Based on the information shown in Fig. 2d, the type-I energy alignment between QD and PCM would not facilitate direct charge transfer from the QD to the PCM. Moreover, previous studies in the literature have shown that direct charge transfer from PbS QD to surface ligands typically occur in the picosecond to few nanosecond time scale[57] which is more than an order of magnitude faster than the PL lifetimes observed in this work, suggesting distinctive mechanisms. Lastly, there is a possibility that the QDs were charged after accepting charges from the excited PCMs during the ultraviolet/visible illumination for configuration switching. We argue that this is not likely because we did not observe any time dependent transient changes in PL intensity within the few hours experiment time periods and our PL results were obtained using near infrared excitation light that does not excite PCMs.

In order to confirm the absence of direct charge transfer from PbS QD to the PCM more directly, we performed a control experiment by employing a mono-esterified PCM (also referred as compound 7 in Scheme S1 of the ESI†) that has the identical chemical structure to the PCM except for an esterified group on one end of the dithienylethene (Fig. 5). Since binding to PbS QD surface occurs through a deprotonated carboxylate by replacing native oleates,[48] the mono-esterified PCM molecule will not cross-link two QDs, thereby eliminating the possibility of inter-QD exciton dissociation mechanism. If the direct charge injection from the QD to the PCM is indeed the dominant non-radiative pathway, then a significant PL quenching from QDs should occur when bound with mono-esterified PCM. The control experiment was conducted using the solution-state QD sample in which the mono-esterified PCMs were added to the QD solution (see the ESI† for the detailed preparation procedure). Conducting the PL measurements with solution samples, instead of solid-state thin film samples, further ensures that the
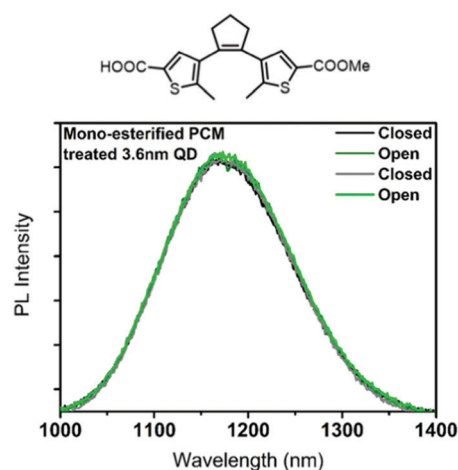

Fig. 5 PL spectra of 3.6 nm QDs with mono-esterified PCMs (compound 7) ligands in "closed" or "open" configuration.

16010 | J. Mater. Chem. C, 2021, 9, 16006–16013

This journal is © The Royal Society of Chemistry 2021

QDs are isolated from each other to better isolate the effect of charge transfer from QDs to surface ligands, if any. Our result (Fig. 5) shows that there is no difference in PL intensity when the mono-esterified PCM is switched between "open" and "closed" state. For direct comparison of this control experiment result with the case of QDs inter-connected with the PCM (compound **6** with carboxylic acid groups on both ends instead of the mono-esterified PCM used in the control experiment), we also performed experiments with solution form samples with addition of PCM at same concentration. In contrast to the mono-esterified PCM experiment, we observed switchable PL intensity from the QD solution samples with PCM depending on the PCM configuration (Fig. S10, ESI†). These results indicate that, with PCM addition, some fractions of QDs become cross-linked by PCMs into dimers, trimers and *etc.* that maintain colloidal stability and the inter-QD exciton dissociation becomes enhanced with the "closed" PCM configuration in those cross linked QD species in solution. In contrast, mono-esterified PCM cannot bridge multiple QDs with each other and the exciton dissociation is not influenced by the configuration of the mono-esterified PCMs. Therefore, these control experiments show that the direct charge transfer from QD to PCM does not occur in these systems but instead the changes in PL intensity observed in this work is due to changes in the amount of excitons going through inter-QD tunnelling and dissociation. In addition, we conclude that, considering the similar physical, chemical and photophysical interactions of the PCM and mono-esterified PCM molecules with PbS QD due to their identical switchable molecular structure and carboxylic acid binding group, various other possibilities such as reversible PbS QD surface modification due to ligand configuration changes and a variety of different energy or charge transfer mechanisms between the ligand molecules and PbS QDs[62,63] are likely not responsible for our results reported in this study.

Conclusions

In summary, this study shows that lowering the inter-QD potential barrier height increases the exciton delocalization and dissociation through tunnelling. This work demonstrates that exploiting the configuration changes of photochromic molecules can provide fertile future directions for QD, molecular electronics and nanoscale charge transfer research communities. For application, the switchable PL intensity from QD found in this work can provide unique opportunities for optical memory and computing technologies. The major challenges facing the current state-of-the-art non-volatile on-chip compatible optical memory materials, such as phase change materials and photochromic molecules, are that phase change materials require large energy light excitations to induce melting[64] and photochromic molecules lack non-destructive readout capabilities due to the readout operation itself causing the switch because both operations use the same wavelength light.[41,42] In contrast, our PCM bridged QD assemblies exhibit near-IR light emission that can be increased or decreased

with UV and visible light exposure. The "read" operations can be performed all in near-IR region that does not cause flipping of PCM configuration. Therefore, the findings in this study can lead to solving the photochromic materials switching their configuration during the "read" operation and provide a new class of materials for non-volatile optical memory and computing applications.

Experimental section

General method and procedure for the photochromic molecules syntheses.

All reactions were carried out under anhydrous conditions at 1 atm, these were typically carried out in flame dried glassware under nitrogen or argon atmosphere. All reagents and solvents were obtained from commercial suppliers such as Sigma-Aldrich, VWR, and Fisher and used directly without any purifications. All reactions unless otherwise noted were carried out in flame dried glassware under nitrogen or argon atmosphere. All purification was conducted by flash chromatography using 230–400 mesh silica gel using gradient solvent systems. Details on the synthesis procedure of molecules are included in the ESI.†

Thin-layer chromatography (TLC) analysis was performed with aluminum backed TLC plates with UV and fluorescence indicator and visualized using UV lamp at 254 nm, then stained with PMA solution. ^{1}H NMR and proton-decoupled ^{13}C NMR spectra were obtained with Bruker 400 MHz spectrometers in DMSO-d_6 or CDCl$_3$. The chemical shifts were reported using CDCl$_3$/DMSO-d_6 as internal standard at 7.26/2.50 ppm and at 77.0/39.5 ppm, respectively. 2D NMR experiments (HSQC, COSY) were also conducted to assist the compound characterizations.

PbS QD synthesis

3 mmol of lead(II) oxide (PbO) (99.999%, Alfa Aesar), 6–96 mmol of oleic acid (HOA) (90%, Sigma Aldrich), and 1-octadecene (90%, Alfa Aesar) were added to make 30 mL total volume in a three-neck flask. To synthesize different sizes of QD (2.9–4.7 nm in diameter), the molar ratio between PbO and HOA was varied from 2:1 to 32:1. The solution was stirred in a vacuumed flask at 130 °C for 1 h until PbO was fully dissolved. Under Argon flow, the temperature was adjusted to 90–95 °C and stabilized prior to the precursor injection. In the N$_2$-filled glovebox, 0.1 M of hexamethyldisilathiane ((TMS)$_2$S) solution was prepared by mixing 378 μL of (TMS)$_2$S in 18 mL of 1-octadecene (ODE). 15 mL of 0.1 M (TMS)$_2$S solution was taken out of the glovebox and quickly injected into the three-neck flask. After 60 s, the reaction flask was put in an ice bath to quickly quench the temperature of the reaction solution. During the purification process, unreacted species were removed by a series of centrifuge steps after cleaning the product with methyl acetate and hexane. The final QD was stored in a solid form in the N$_2$ glovebox.

PCM treated PbS QD assembly preparation

Solutions of 10 mg mL^{-1} concentration of PbS QD in tetrachloroethylene (TCE) and 1.8 mM of PCM in methanol (MeOH)

This journal is © The Royal Society of Chemistry 2021

J. Mater. Chem. C, 2021, **9**, 16006–16013 | **16011**

were prepared and stirred overnight in the N_2 glovebox prior to use. The glass substrates were sequentially cleaned by sonicating in Hellmanex soap solution, deionized water, iso-propanol and then acetone. Subsequently, the clean substrates were UV-ozone treated for 10 min. In the glovebox, 100 μL of PbS QD solution was statically dispensed onto the glass substrate, followed by a spin-coating at 2000 rpm for 60 s. Ligand exchange was done by placing 100 μL of the PCM solution onto the QD thin film for 60 s. The process was repeated two more times. The film was rinsed with MeOH to remove any unbound excess ligands. The film was encapsulated with a glass slide using epoxy curing to prevent any complications from exposure to ambient air.

Absorbance, photoluminescence (PL), time-resolved photoluminescence (TR-PL) and Raman spectroscopy measurements

Absorbance measurement was performed using PerkinElmer Lambda 950S spectrophotometer equipped with an integrating sphere. PL measurements were taken using PTI Quantamaster 400 system. Time-resolved PL was taken with a time correlated single photon counting set-up with a pulsed 633 nm laser diode as the excitation light source. Time-resolved PL measurements were taken at the peak PL emission wavelength of the QD samples (1080 nm, 1200 nm, 1380 nm for 2.9 nm QD, 3.6 nm QD and 4.7 nm QD respectively). Raman spectroscopy measurement was performed using Renishaw Raman microscope with 514 nm laser as an excitation source and a 50× objective to focus the laser on the sample.

PL measurements on PCM treated QD samples

The encapsulated PCM treated QD thin film samples were placed on the stage in the spectrofluorometer. The light wavelength was changed to 300 nm or 541 nm to induce the configuration change of PCM. After inducing the configuration change of PCMs, without changing the position of the sample or any other parts of the setup, the excitation light wavelength was changed to 750 nm to obtain the PL spectra from QDs. All instrumental parameters such as slit widths, detector voltage, stage angle and *etc.* were kept constant throughout the measurements.

GISAXS measurement

GISAXS characterizations were performed at the 11-BM Complex Materials Scattering (CMS) beamline at the National Synchrotron Light Source II (NSLS-II) in the Brookhaven National Laboratory. Thin film samples were measured at incident angles from 0.10 to 0.25° with a 200 μm (H) × 50 μm (V) beam at 13.5 keV (wavelength λ = 0.9184 Å). 2D scattering patterns were obtained using Dectris Pilatus 2M at 2 m downstream the samples.

Solution-state PCM and mono-esterified PCM treated PbS QD sample preparation

10 mg mL^{-1} concentration of PbS QD in tetrachloroethylene (TCE) and 1.8 mM of PCM or mono-esterified PCM in methanol (MeOH) were prepared and mixed to yield a molar ratio of 1 QD : 100 PCM. The prepared solution was then stirred in a N_2

glovebox environment overnight. The solution was transferred to a 10 mm cuvette with an air-tight cap to minimize ambient exposure for optical measurements.

Author contributions

J. J. C. and G. W. conceived and designed the research. L. U. Y., S. B. A., E. S. S., J. M. B., E. H. R. T. performed experiments. All authors contributed to data analysis. L. U. Y., G. W. and J. J. C. wrote the manuscript.

Conflicts of interest

There are no conflicts to declare.

Acknowledgements

References

1 P. V. Kamat, *J. Phys. Chem. C*, 2008, **112**, 18737–18753.
2 V. I. Klimov, *Annu. Rev. Phys. Chem.*, 2007, **58**, 635–673.
3 C. B. Murray, A. C. Kagan and M. Bawendi, *Annu. Rev. Mater. Sci.*, 2000, **30**, 545–610.
4 A. J. Nozik, M. C. Beard, J. M. Luther, M. Law, R. J. Ellingson and J. C. Johnson, *Chem. Rev.*, 2010, **110**, 6873–6890.
5 D. V. Talapin, J.-S. Lee, M. V. Kovalenko and E. V. Shevchenko, *Chem. Rev.*, 2010, **110**, 389–458.
6 J. Tang and E. H. Sargent, *Adv. Mater.*, 2011, **23**, 12–29.
7 F. W. Wise, *Acc. Chem. Res.*, 2000, **33**, 773–780.
8 L. E. Brus, *J. Chem. Phys.*, 1984, **80**, 4403–4409.
9 A. I. Ekimov, A. L. Efros and A. A. Onushchenko, *Solid State Commun.*, 1985, **56**, 921–924.
10 K. Bian, J. J. Choi, A. Kaushik, P. Clancy, D.-M. Smilgies and T. Hanrath, *ACS Nano*, 2011, **5**, 2815–2823.
11 Q. Chen, S. C. Bae and S. Granick, *Nature*, 2011, **469**, 381–384.
12 J. J. Choi, C. R. Bealing, K. Bian, K. J. Hughes, W. Zhang, D.-M. Smilgies, R. G. Hennig, J. R. Engstrom and T. Hanrath, *J. Am. Chem. Soc.*, 2011, **133**, 3131–3138.
13 J. J. Choi, K. Bian, W. J. Baumgardner, D.-M. Smilgies and T. Hanrath, *Nano Lett.*, 2012, **12**, 4791–4798.
14 P. F. Damasceno, M. Engel and S. C. Glotzer, *Science*, 2012, **337**, 453–457.
15 A. Dong, J. Chen, P. M. Vora, J. M. Kikkawa and C. B. Murray, *Nature*, 2010, **466**, 474–477.

16012 | *J. Mater. Chem. C*, 2021, **9**, 16006–16013

This journal is © The Royal Society of Chemistry 2021

16 G. Markovich, C. P. Collier, S. E. Henrichs, F. Remacle, R. D. Levine and J. R. Heath, *Acc. Chem. Res.*, 1999, **32**, 415–423.

17 S. A. Claridge, A. Castleman Jr, S. N. Khanna, C. B. Murray, A. Sen and P. S. Weiss, *ACS Nano*, 2009, **3**, 244–255.

18 E. Bakkers, A. Roest, A. Marsman, L. Jenneskens, L. De Jong-Van Steensel, J. Kelly and D. Vanmaekelbergh, *J. Phys. Chem. B*, 2000, **104**, 7266–7272.

19 J. E. Murphy, M. C. Beard and A. J. Nozik, *J. Phys. Chem. B*, 2006, **110**, 25455–25461.

20 I. Mora-Seró, S. Giménez, T. Moehl, F. Fabregat-Santiago, T. Lana-Villareal, R. Gómez and J. Bisquert, *Nanotechnology*, 2008, **19**, 424007.

21 A. Zabet-Khosousi and A.-A. Dhirani, *Chem. Rev.*, 2008, **108**, 4072–4124.

22 Y. Liu, M. Gibbs, J. Puthussery, S. Gaik, R. Ihly, H. W. Hillhouse and M. Law, *Nano Lett.*, 2010, **10**, 1960–1969.

23 M. H. Zarghami, Y. Liu, M. Gibbs, E. Gebremichael, C. Webster and M. Law, *ACS Nano*, 2010, **4**, 2475–2485.

24 B.-R. Hyun, A. Bartnik, L. Sun, T. Hanrath and F. Wise, *Nano Lett.*, 2011, **11**, 2126–2132.

25 J. Tang, K. W. Kemp, S. Hoogland, K. S. Jeong, H. Liu, L. Levina, M. Furukawa, X. Wang, R. Debnath and D. Cha, *Nat. Mater.*, 2011, **10**, 765–771.

26 Y. Gao, M. Aerts, C. S. Sandeep, E. Talgorn, T. J. Savenije, S. Kinge, L. D. Siebbeles and A. J. Houtepen, *ACS Nano*, 2012, **6**, 9606–9614.

27 K. S. Jeong, J. Tang, H. Liu, J. Kim, A. W. Schaefer, K. Kemp, L. Levina, X. Wang, S. Hoogland and R. Debnath, *ACS Nano*, 2012, **6**, 89–99.

28 J. J. Choi, J. Luria, B.-R. Hyun, A. C. Bartnik, L. Sun, Y.-F. Lim, J. A. Marohn, F. W. Wise and T. Hanrath, *Nano Lett.*, 2010, **10**, 1805–1811.

29 L. Sun, J. J. Choi, D. Stachnik, A. C. Bartnik, B.-R. Hyun, G. G. Malliaras, T. Hanrath and F. W. Wise, *Nat. Nanotechnol.*, 2012, **7**, 369–373.

30 J. J. Choi, Y.-F. Lim, M. E. B. Santiago-Berrios, M. Oh, B.-R. Hyun, L. Sun, A. C. Bartnik, A. Goedhart, G. G. Malliaras and H. D. Abruna, *Nano Lett.*, 2009, **9**, 3749–3755.

31 J. M. Luther, M. Law, M. C. Beard, Q. Song, M. O. Reese, R. J. Ellingson and A. J. Nozik, *Nano Lett.*, 2008, **8**, 3488–3492.

32 J. M. Luther, M. Law, Q. Song, C. L. Perkins, M. C. Beard and A. J. Nozik, *ACS Nano*, 2008, **2**, 271–280.

33 G. I. Koleilat, L. Levina, H. Shukla, S. H. Myrskog, S. Hinds, A. G. Pattantyus-Abraham and E. H. Sargent, *ACS Nano*, 2008, **2**, 833–840.

34 A. T. Fafarman, W.-k. Koh, B. T. Diroll, D. K. Kim, D.-K. Ko, S. J. Oh, X. Ye, V. Doan-Nguyen, M. R. Crump and D. C. Reifsnyder, *J. Am. Chem. Soc.*, 2011, **133**, 15753–15761.

35 W.-k. Koh, S. R. Saudari, A. T. Fafarman, C. R. Kagan and C. B. Murray, *Nano Lett.*, 2011, **11**, 4764–4767.

36 M. V. Kovalenko, M. Scheele and D. V. Talapin, *Science*, 2009, **324**, 1417–1420.

37 J.-S. Lee, M. V. Kovalenko, J. Huang, D. S. Chung and D. V. Talapin, *Nat. Nanotechnol.*, 2011, **6**, 348–352.

38 A. Nag, M. V. Kovalenko, J.-S. Lee, W. Liu, B. Spokoyny and D. V. Talapin, *J. Am. Chem. Soc.*, 2011, **133**, 10612–10620.

39 T. Fukaminato, S. Ishida and R. Métivier, *NPG Asia Mater.*, 2018, **10**, 859–881.

40 M. Irie, *Photochem. Photobiol. Sci.*, 2010, **9**, 1535–1542.

41 M. Irie, *Chem. Rev.*, 2000, **100**, 1685–1716.

42 H. Tian and S. Yang, *Chem. Soc. Rev.*, 2004, **33**, 85–97.

43 J. Zhang, Q. Zou and H. Tian, *Adv. Mater.*, 2013, **25**, 378–399.

44 G. Guirado, C. Coudret, M. Hliwa and J.-P. Launay, *J. Phys. Chem. B*, 2005, **109**, 17445–17459.

45 J. Owrutsky, H. Nelson, A. Baronavski, O.-K. Kim, G. Tsivgoulis, S. Gilat and J.-M. Lehn, *Chem. Phys. Lett.*, 1998, **293**, 555–563.

46 J. Jasieniak, M. Califano and S. E. Watkins, *ACS Nano*, 2011, **5**, 5888–5902.

47 S. Padgaonkar, C. T. Eckdahl, J. K. Sowa, R. López-Arteaga, D. E. Westmoreland, E. F. Woods, S. Irgen-Gioro, B. Nagasing, T. Seideman and M. C. Hersam, *Nano Lett.*, 2021, **21**, 854–860.

48 N. C. Anderson, M. P. Hendricks, J. J. Choi and J. S. Owen, *J. Am. Chem. Soc.*, 2013, **135**, 18536–18548.

49 J. R. Lakowicz, *Principles of fluorescence spectroscopy*, Springer science & business media, 2013.

50 Z. Lingley, S. Lu and A. Madhukar, *J. Appl. Phys.*, 2014, **115**, 084302.

51 L. Dworak, A. J. Reuss, M. Zastrow, K. Rück-Braun and J. Wachtveitl, *Nanoscale*, 2014, **6**, 14200–14203.

52 N. Yano, M. Yamauchi, D. Kitagawa, S. Kobatake and S. Masuo, *J. Phys. Chem. C*, 2020, **124**, 17423–17429.

53 Y. Seto, R. Yamada, D. Kitagawa, D. Kim and S. Kobatake, *Chem. Lett.*, 2019, **48**, 1394–1397.

54 Y. Akaishi, A. D. Pramata, S. Tominaga, S. Kawashima, T. Fukaminato and T. Kida, *Chem. Commun.*, 2019, **55**, 8060–8063.

55 V. Krivenkov, P. Samokhvalov, M. Zvaigzne, I. Martynov, A. Chistyakov and I. Nabiev, *J. Phys. Chem. C*, 2018, **122**, 15761–15771.

56 S. Saeed, J. Yin, M. A. Khalid, P. A. Channar, G. Shabir, A. Saeed, M. A. Nadeem, C. Soci and A. Iqbal, *J. Photochem. Photobiol., A*, 2019, **375**, 48–53.

57 K. E. Knowles, M. D. Peterson, M. R. McPhail and E. A. Weiss, *J. Phys. Chem. C*, 2013, **117**, 10229–10243.

58 R. D. Harris, S. Bettis Homan, M. Kodaimati, C. He, A. B. Nepomnyashchii, N. K. Swenson, S. Lian, R. Calzada and E. A. Weiss, *Chem. Rev.*, 2016, **116**, 12865–12919.

59 M. D. Peterson, L. C. Cass, R. D. Harris, K. Edme, K. Sung and E. A. Weiss, *Annu. Rev. Phys. Chem.*, 2014, **65**, 317–339.

60 G. M. Akselrod, P. B. Deotare, N. J. Thompson, J. Lee, W. A. Tisdale, M. A. Baldo, V. M. Menon and V. Bulović, *Nat. Commun.*, 2014, **5**, 1–8.

61 R. H. Gilmore, E. M. Lee, M. C. Weidman, A. P. Willard and W. A. Tisdale, *Nano Lett.*, 2017, **17**, 893–901.

62 J. B. Hoffman, H. Choi and P. V. Kamat, *J. Phys. Chem. C*, 2014, **118**, 18453–18461.

63 Z. Xu, Z. Huang, T. Jin, T. Lian and M. L. Tang, *Acc. Chem. Res.*, 2020, **54**, 70–80.

64 C. Ríos, M. Stegmaier, P. Hosseini, D. Wang, T. Scherer, C. D. Wright, H. Bhaskaran and W. H. P. Pernice, *Nat. Photonics*, 2015, **9**, 725–732.

This journal is © The Royal Society of Chemistry 2021

J. Mater. Chem. C, 2021, **9**, 16006–16013 | **16013**